Protonation Structures of Cys-Sulfinic and Cys-Sulfenic Acids in the Photosensitive Nitrile Hydratase Revealed by Fourier Transform Infrared Spectroscopy†

Takumi Noguchi,*,‡ Masaki Nojiri,§,|| Ken-ichi Takei,‡ Masafumi Odaka,⊥ and Nobuo Kamiya§

Institute of Materials Science, University of Tsukuba, Tsukuba, Ibaraki 305-8573, Japan, RIKEN Harima Institute/SPring-8, Mikazuki-cho, Sayou-gun, Hyogo 679-5148, Japan, and Bioengineering Laboratory, RIKEN, Wako, Saitama 351-0198, Japan

Received July 17, 2003; Revised Manuscript Received August 12, 2003

ABSTRACT: Nitrile hydratase (NHase) from *Rhodococcus* N-771, which catalyzes hydration of nitriles to the corresponding amides, exhibits novel photosensitivity; in the dark, it is in the inactive form that binds an endogenous nitric oxide (NO) molecule at the non-heme iron center, and photodissociation of the NO activates the enzyme. NHase is also known to have a unique active site structure. Two cysteine ligands to the iron center, αCys112 and αCys114, are post-translationally modified to sulfinic acid (Cys-SO_2H) and sulfenic acid (Cys-SOH), respectively, which are thought to play a crucial role in the catalytic reaction. Here, we have determined the protonation structures of these Cys-SO_2H and Cys-SOH groups using Fourier transform infrared (FTIR) spectroscopy in combination with density functional theory (DFT) calculations. The light-induced FTIR difference spectrum of NHase between the dark inactive and light active forms exhibited two prominent signals at (1154−1148)/1126 and (1040−1034)/1019 cm^{-1}, which downshifted to 1141/1114 and 1026/1012 cm^{-1}, respectively, in the uniformly ^{34}S-labeled NHase. In addition, a minor signal at 915/908 cm^{-1} also showed a considerable downshift upon ^{34}S labeling. These ^{34}S-sensitive signals were basically conserved in D_2O buffer with only slight shifts. Vibrational frequencies of methanesulfenic acid (CH_3SOH) and methanesulfinic acid (CH_3SO_2H), simple model compounds of Cys-SOH and Cys-SO_2H, respectively, were calculated using the DFT method in both the protonated and deprotonated forms and in metal complexes. Comparison of the calculated frequencies and isotope shifts with the observed ones provided the assignment of the two major signals around 1140 and 1030 cm^{-1} to the asymmetric and symmetric SO_2 stretching vibrations, respectively, of the S-bonded Cys-SO_2^- complex, and the assignment of the minor signal around 910 cm^{-1} most likely to the SO stretch of the S-bonded Cys-SO^- complex. These assignments and the small frequency shifts upon deuteration are consistent with the view that the deprotonated αCys112-SO_2^- and αCys114-SO^- are hydrogen-bonded with the protons from βArg56 and/or βArg141, forming a reactive cavity at the interface of the α and β subunits. There is further speculation that either of these groups is hydrogen bonded to a reactant water molecule, increasing its basicity to facilitate the nucleophilic attack on the nitrile substrate bound to the iron center.

Nitrile hydratases (NHases)[1] are bacterial enzymes that catalyze the hydration of nitriles to the corresponding amides. They have been used in the industrial production of acrylamide and nicotinamide, and are also important for bioremediation in which nitriles in industrial waste and toxic herbicides can be degraded (*1*−*3*). There are two types of NHases that contain either a non-heme iron(III) center (Fe-type NHase) or a noncorrinoid cobalt(III) center (Co-type NHase). They consist of α and β subunits and are significantly homologous in protein sequences even between the Fe- and Co-type NHases (*1*).

Some of the Fe-type NHases, those from *Rhodococcus* N-774, N-771, and R312, exhibit a characteristic phenomenon of photoactivation; that is, they are inactive in the dark and activated by light illumination (*4*, *5*). FTIR, resonance Raman, and ESR spin trapping measurements uncovered the photoactivation mechanism in which an endogenous nitric oxide (NO) molecule is bound to the iron center in the dark inactive NHase and photodissociation of NO converts it to the active form (*6*−*8*). It was also shown that the Fe-type NHase from *Comamonas testosteroni* NI1, which does not exhibit photosensitivity originally, was inactivated by exogenous NO and reactivated by subsequent light illumination (*9*). The X-ray crystal structure (*10*) as well as the iron K-edge X-ray absorption spectrum (*11*) of the dark inactive NHase further confirmed the presence of an NO molecule bound to the iron center.

† This study was supported by a Grant-in-Aid for Scientific Research (14540607) from the Ministry of Education, Culture, Sports, Science and Technology of Japan and by Special Research Project "Nano-Science" at the University of Tsukuba.

* To whom correspondence should be addressed. Phone: +81-29-853-5126. Fax: +81-29-855-7440. E-mail: tnoguchi@ims.tsukuba.ac.jp.

‡ University of Tsukuba.

§ RIKEN Harima Institute/SPring-8.

|| Present address: Osaka University, Toyonaka, Osaka 560-0043, Japan.

⊥ RIKEN.

[1] Abbreviations: Cys-SOH, cysteinesulfenic acid; Cys-SO_2H, cysteinesulfinic acid; DFT, density functional theory; FTIR, Fourier transform infrared; IR, infrared; NHase, nitrile hydratase; *R.*, *Rhodococcus*.

10.1021/bi035260i CCC: $25.00
Published on Web 09/20/2003

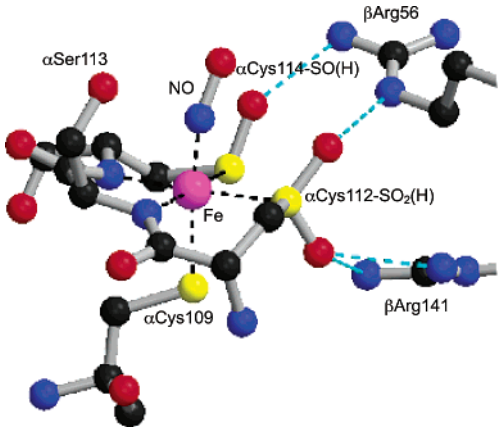

FIGURE 1: Structure of the non-heme iron center of dark inactive NHase of *R.* N-771 (*10*). Atoms are shown with different colors: magenta for Fe, black for C, red for O, yellow for S, and blue for N.

The non-heme iron of the light active NHase is in a low-spin Fe(III) state (*12*, *13*). Its protein ligands were first revealed in the crystal structure of the active NHase at 2.65 Å resolution by Huang et al. (*14*) as three S atoms of cysteine side chains and two nitrogen atoms of backbone amides, being consistent with earlier spectroscopic results from ESR (*12*), ENDOR (*15*, *16*), EXAFS (*17*, *18*), and resonance Raman (*17*, *19*) experiments. Subsequently, the crystal structure of the dark inactive NHase at 1.7 Å resolution determined by Nagashima et al. (*10*) along with the information from mass spectrometry (*20*) showed that two of the three cysteine ligands, αCys112 and αCys114, are post-translationally modified to cysteinesulfinic acid (Cys-SO_2H) and cysteinesulfenic acid (Cys-SOH), respectively. These sulfinic and sulfenic acids interact with *β*Arg56 and *β*Arg141, forming a reactive cavity at the interface of the α and *β* subunits (Figure 1). Although direct evidence for the presence of sulfenic acid at αCys114 is yet to be obtained in light active NHase (*14*, *21*, *22*), the crystal structure of the Co-type NHase from *Pseudonocardia thermophila* JCM 3095, which neither possesses NO nor exhibits photosensitivity, also showed that two cysteine ligands, αCys111 and αCys113, are modified to sulfinic and sulfenic acids, respectively (*23*).

Post-translationally modified Cys-SOH and Cys-SO_2H are known to play key roles in catalytic mechanisms and activity regulation in various proteins such as NADH peroxidase and peroxiredoxins (*24*−*29*). Among them, NHase is an especially unique enzyme that possesses both Cys-SOH and Cys-SO_2H as ligands of the metal center. These sufenic and sulfinic groups are also indispensable to the catalytic function of NHase. When NHase was reconstituted from the recombinant α and *β* subunits in the presence of ferric ions, the enzyme was first inactive under an anaerobic condition but became active after aerobic incubation, which induced oxidation of αCys112 and αCys114 to Cys-SO_2H and Cys-SOH, respectively (*21*). However, further aerobic incubation gradually decreased the activity probably because αCys114-SOH was excessively oxidized to Cys-SO_2H (*21*). Recent kinetic analysis has shown that an irreversible inhibitor, 2-cyano-2-propyl hydroperoxide, inactivates NHase by oxidizing αCys114-SOH to Cys-SO_2H (*30*). Thus, αCys112-SO_2H and αCys114-SOH should be directly or indirectly involved in the catalytic reactions of nitrile hydration, and hence, studying the structure and molecular interactions of the sulfenic and sulfinic groups in the active site is crucial in clarifying the reaction mechanism. To date, however, even the basic questions such as whether these groups have protonated SO_2H and SOH forms or deprotonated sulfinate (SO_2^-) and sulfenate (SO^-) forms have not been answered, because the X-ray crystal structure analysis of inactive NHase at 1.7 Å resolution (*10*) could neither resolve hydrogen atoms nor determine the S−O distances as accurately as it could distinguish the protonation structures. The protonation structures of these groups are particularly important in the relevance to the active site structure, including the binding sites and hydrogen bonding interactions of a nitrile substrate and a reactant water, which are essential for the mechanism of the enzymatic reaction of NHase.

Vibrational spectroscopies, including infrared absorption and resonance Raman scattering, are powerful methods for detecting protonation structures and hydrogen bonding interactions in proteins. These spectroscopies are even more important after the X-ray crystal structures of proteins are available, because they provide detailed information about the chemical bonds and interactions in the active sites, which is often not obtained by X-ray crystallography but is essential in clarifying the enzymatic mechanism. In particular, FTIR difference spectroscopy is suitable for detecting the structures of protein side chains in the catalytic center coupled to some reaction. In this study, the protonation structures and interactions of Cys112-SO_2H and Cys114-SOH in the photosensitive NHase from *R.* N-771 were studied by means of light-induced FTIR difference spectroscopy in combination with uniform ^{34}S isotope labeling and vibrational analysis using density functional theory (DFT) calculations.

MATERIALS AND METHODS

Dark inactive NHase was purified from *R.* N-771 cells as described previously (*31*). For uniform ^{34}S isotope labeling of NHase, *R.* N-771 cells were cultured in a growth medium containing 4% glucose, 42 mM Na_2HPO_4, 22 mM KH_2PO_4, 60 mM NH_4Cl, 75 mM NH_4NO_3, 2 mM $MgCl_2$, 1 mM $FeCl_3$, 0.1 mM $CaCl_2$, and 0.044 mM thiamine-HCl in the presence of 10 mM $(NH_4)_2{}^{34}SO_4$ (Shoko Co., ∼90 at. % ^{34}S) as a sulfur source.

The NHase sample (∼200 mg/mL, 1 *μ*L) in 50 mM Tris-HCl buffer (pH 7.5), including 20 mM butyric acid, was placed between two BaF_2 plates (*ϕ* of 13 mm). The sample temperature was adjusted to 250 K in a cryostat (Oxford DN-1704) using a temperature controller (Oxford ITC-5).

Light-induced FTIR difference spectra were recorded using a Bruker IFS-66/S spectrophotometer equipped with an MCT detector (InfraRed D316/8). A Ge filter (OCLI LO2584-9) was placed in front of the sample to cut the He−Ne laser beam from the interferometer. Single-beam spectra of 600 scans (150 s) with a single-sided forward−backward mode were recorded before and after illumination for 10 s by continuous white light from a halogen lamp (Hoya-Shott HL150), and a light minus dark difference spectrum was calculated. The light intensity was approximately 60 mW/cm^2 at the sample surface.

The FTIR spectrum of sodium methanesulfinate (CH_3SO_2-Na) (Wako Pure Chemical Industries, Ltd., Osaka, Japan)

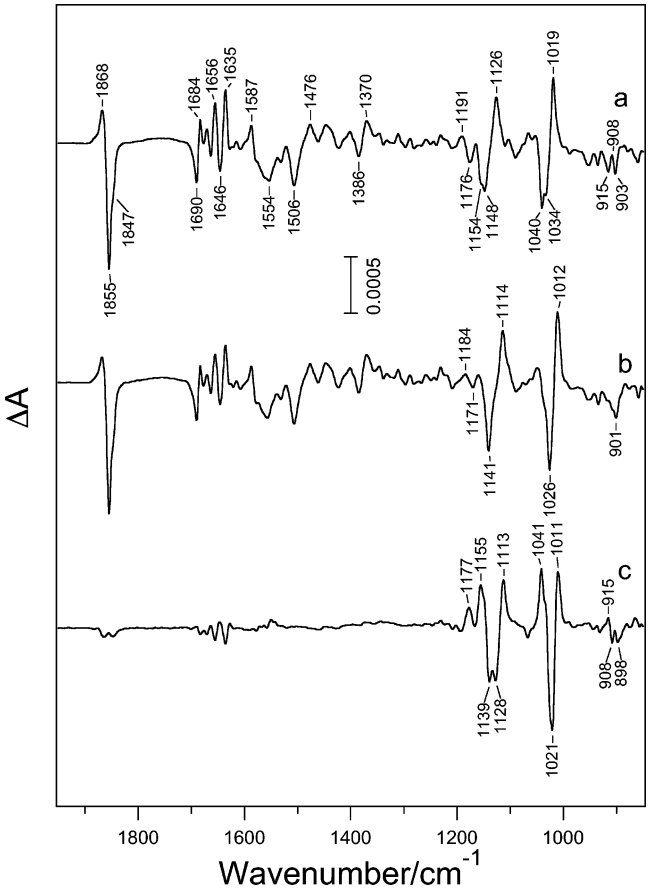

FIGURE 2: Light-induced FTIR difference spectra (active minus inactive form) of (a) unlabeled NHase and (b) uniformly ^{34}S-labeled NHase. (c) ^{34}S minus ^{32}S double-difference spectrum (b minus a). Spectra were recorded at 250 K. Spectrum b was scaled to adjust the NO intensity at 1855 cm^{-1} to that of spectrum a.

in a solid state was measured at room temperature using an ATR accessory (DuraSamplIR II; SensIR Technologies) with a 3 mm silicon window. All FTIR spectra were measured with a resolution of 4 cm^{-1}.

Ab initio MO calculations were performed with the GAUSSIAN 98 program package (*32*). The geometry optimizations were carried out by the DFT method using Becke's three-parameter hybrid functional (*33*) combined with the Lee−Yang−Parr correlation functional (B3LYP) (*34*) with the 6-31G(d,p) basis set except for Zn and Co atoms, for which the Hay−Wadt effective core potential (LANL2DZ) was used. The Cartesian force constants and the vibrational frequencies were analytically computed at the fully optimized geometries. The obtained force constant matrix was transformed from Cartesian to internal coordinates, and the potential energy distributions were calculated using a modified version of the NCTB program (*35*). The computed frequencies were not scaled. IR intensities were computed in the GAUSSIAN program.

RESULTS

Light-Induced FTIR Difference Spectra of Unlabeled and ^{34}S-Labeled NHase. Figure 2a shows a light-induced FTIR spectrum (after minus before illumination) of NHase in the region of 1950−850 cm^{-1}. The spectrum reflects the structural changes of NHase upon photoactivation, and hence, the negative and positive peaks belong to the dark inactive and light active forms of NHase, respectively. The large negative band at 1855 cm^{-1} with a shoulder at 1847 cm^{-1} arises from the stretching mode of the NO molecule bound to the non-heme iron of the inactive NHase (*6*). Bands in the frequency region lower than 1700 cm^{-1} are due to the vibrations of protein backbones and side chains. Prominent features in the regions of 1700−1600 and 1600−1500 cm^{-1} are probably from the amide I (C═O stretch) and II (NH deformation coupled to C−N stretch) modes, respectively, of backbone amides (*36*, *37*), which appear by perturbations of protein conformations upon photoactivation. In addition, the asymmetric and symmetric stretches of the guanidinium ($CN_3H_5^+$) groups of Arg residues (*38*) are expected to be present in the 1700−1600 cm^{-1} region, because the crystal structure of NHase showed the interactions of βArg56 and βArg141 with the iron center through the αCys112-SO_2H and αCys114-SOH ligands (*10*). In the 1200−1000 cm^{-1} region, two prominent signals were observed: negative doublet peaks at 1154 and 1148 cm^{-1} with a positive peak at 1126 cm^{-1} and another negative doublet at 1040 and 1034 cm^{-1} with a positive peak at 1019 cm^{-1}. There is also a minor signal at 1191(+)/1176(−) cm^{-1} (the − and + signs in parentheses indicate negative and positive intensities, respectively). In the lower-frequency region, several small peaks appeared at 953(−)/943(+)/935(−)/929(+)/915(−)/908(+)/903(−) cm^{-1}. The present FTIR spectrum does not cover the region of the iron−ligand vibrations, including the Fe−NO and Fe−S stretches that occur at frequencies lower than 800 cm^{-1} (*7*, *17*, *19*). The minor positive peak at 1868 cm^{-1} also arises from a NO vibration (*6*). Although this peak was previously interpreted as being due to the NO molecule released from the iron center and then bound to the nonspecific site of the protein (*8*), our recent preliminary data suggest that this peak together with a minor differential signal at 1191/1176 cm^{-1} seems to originate from nitrosylation of the contaminating NHase in which the Cys-SOH is further oxidized to Cys-SO_2H (T. Noguchi, unpublished observations). Note that although the buffer used in this study includes 20 mM butyric acid, which has been used as a protein stabilizer but was recently found to work as a competitive inhibitor in the active form of NHase (*39*), the light-induced FTIR spectrum of NHase in the absence of butyric acid (data not shown) was basically identical to the spectrum in Figure 2a and the peak frequencies agreed within a few wavenumbers. For instance, the prominent peaks in the 1200−1000 cm^{-1} region were observed at 1155, 1147, 1124, 1040, 1033, and 1018 cm^{-1} in the buffer without butyric acid. Further careful studies using isotope-labeled butyric acid are necessary to elucidate the effect of butyric acid on the FTIR spectrum.

When sulfur atoms (natural abundance ^{32}S) of NHase were uniformly labeled with ^{34}S, the bands at the frequencies lower than 1200 cm^{-1} were largely affected, whereas changes were hardly seen in the higher-frequency region (Figure 2b). This ^{34}S effect is more obvious in the ^{34}S minus ^{32}S double-difference spectrum (Figure 2c); virtually all the bands in 1900−1200 cm^{-1} region were canceled, while prominent signals were left in the 1200−1000 cm^{-1} region together with minor but meaningful peaks around 900 cm^{-1}. Note that small residual peaks in the 1700−1600 cm^{-1} regions are probably due to the amide I bands, whose intensities are

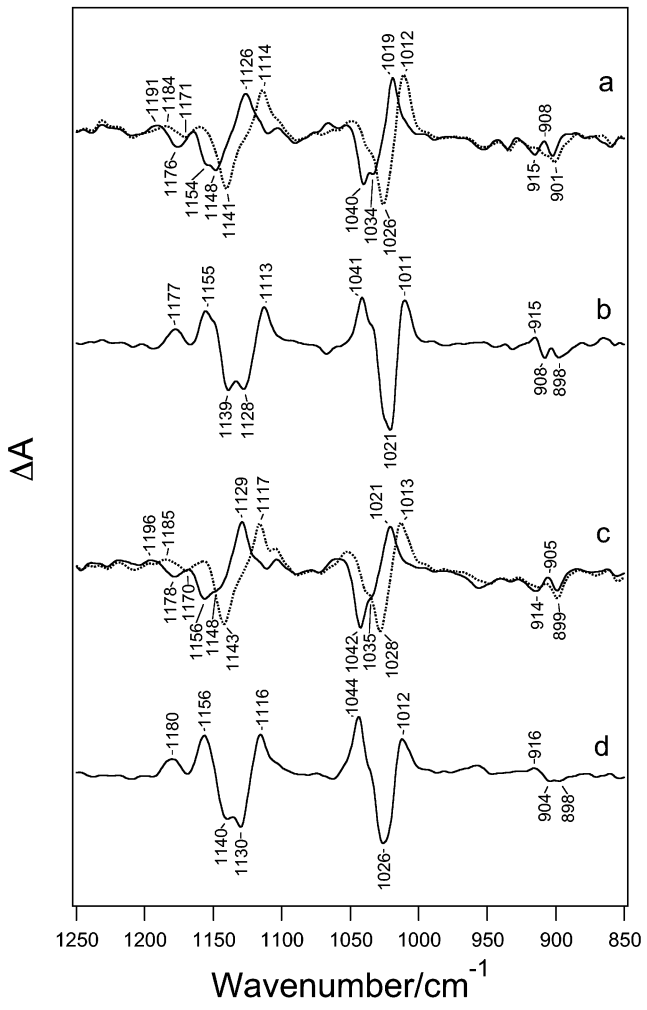

FIGURE 3: Expanded view (1250−850 cm^{-1}) of the ^{34}S-sensitive region of the FTIR difference spectra of unlabeled (—) and ^{34}S-labeled (···) NHase in H_2O buffer (a) and in D_2O buffer (c), and the double-difference spectra (^{34}S minus ^{32}S) for H_2O buffer (b) and D_2O buffer (d).

highly sensitive to the sample condition and hence often change from sample to sample. The expanded view of the ^{34}S-sensitive region of the unlabeled (solid line) and ^{34}S-labeled (dotted line) spectra is presented in Figure 3a. The major signal at (1154−1148)(−)/1126(+) cm^{-1} downshifted to 1141(−)/1114(+) cm^{-1} by (7−13)/12 cm^{-1}, and similarly, the signal at (1040−1034)(−)/1019(+) cm^{-1} downshifted to 1026(−)/1012(+) cm^{-1} by (8−14)/7 cm^{-1} (Figure 3a). It is noted that the doublet peaks at 1154 and 1148 cm^{-1} and at 1040 and 1034 cm^{-1} are probably due to Fermi resonance rather than heterogeneity of the NHase sample, because both the doublets were changed to singlets upon ^{34}S labeling (Figure 3a) and also the latter doublet becomes a singlet upon ^{15}N labeling (*6*). Along with the shifts of these prominent signals, a negative peak at 915 cm^{-1} clearly downshifted to ∼901 cm^{-1} by ∼14 cm^{-1} (Figure 3a). Since the ^{34}S minus ^{32}S double-difference spectrum (Figure 3b) exhibited a clear peak at 908 cm^{-1}, the positive peak at this position in the unlabeled NHase spectrum (Figure 3a, solid line) is probably the counter peak of the negative peak at 915 cm^{-1}, although the corresponding peak in the ^{34}S spectrum was not clearly identified even in the double-difference spectrum (Figure 3b).

Unlabeled and ^{34}S-labeled NHase in D_2O buffer (Figure 3c, solid and dotted lines, respectively) exhibited spectral features very similar to those in H_2O buffer in the 1250−850 cm^{-1} region. The two prominent differential signals, however, upshifted in a parallel way by 2−3 cm^{-1} on average, and showed frequencies at (1156−1148)(−)/1129(+) and (1042−1035)(−)/1021(+) cm^{-1} for the unlabeled sample and at 1143(−)/1117(+) and 1028(−)/1013(+) cm^{-1} for the ^{34}S-labeled sample. These parallel shifts are reflected well in the ^{34}S minus ^{32}S double-difference spectra; the shapes of two prominent signals at 1155(+)/1139(−)/1128(−)/1113(+) and 1041(+)/1021(−)/1011(+) cm^{-1} in H_2O (Figure 3b) are conserved in D_2O but at slightly (1−5 cm^{-1}) upshifted positions of 1156(+)/1140(−)/1130(−)/1116(+) and 1044(+)/1026(−)/1012(+) cm^{-1}, respectively (Figure 3d). Note that minor positive peaks in the double-difference spectra at 1177 cm^{-1} in H_2O and at 1180 cm^{-1} in D_2O are due to the peaks probably related to the excessively oxidized NHase (see above).

Another ^{34}S-sensitive signal at 915(−)/908(+) cm^{-1} (Figure 3a, solid line) was also conserved in D_2O at 914(−)/905(+) cm^{-1} (Figure 3c, solid line). The double-difference spectrum exhibits peaks at 916(+)/904(−)/898(−) cm^{-1} in D_2O (Figure 3d) corresponding to the peaks at 915(+)/908(−)/898(−) cm^{-1} in H_2O (Figure 3b), indicating that the similar ^{34}S-induced shifts took place in D_2O.

DFT Calculations of the Vibrational Frequencies of the Protonated and Deprotonated Forms of Sulfenic and Sulfinic Acids. To analyze the ^{34}S-sensitive bands in the FTIR difference spectra of NHase, normal mode vibrations of the protonated and deprotonated forms of methanesulfenic acid (CH_3SOH and CH_3SO^-) and methanesulfinic acid (CH_3SO_2H and $CH_3SO_2^-$), as the simple model compounds of Cys-SO(H) and Cys-SO_2(H), respectively, were calculated using the *ab initio* DFT method. Vibrations of metal complexes with an S-bonded sulfenate or sulfinate ligand were also calculated. As a metal ion, Zn^{2+} or low-spin Co^{3+} was selected rather than a ferric ion in the Fe-type NHase, because of the closed shell configuration with a singlet spin state that considerably facilitates the process of geometry optimization. In addition, a low-spin Co^{3+} ion works as a metal center in the Co-type NHase that possesses the Cys-SO_2H and Cys-SOH ligands (*23*). A tetrahedral coordination of Zn^{2+} with chloride anions as other ligands and an octahedral coordination of Co^{3+} with cyanide ligands were assumed as model systems for calculations.

Figure 4 presents the optimized geometries of CH_3SOH and its related compounds, and Table 1 summarizes the calculated frequencies of the selected vibrations of the sulfenic groups. The calculated frequencies of CH_3SOH showed the SOH deformation (δSOH) and the SO stretching (νSO) vibrations at 1199 and 756 cm^{-1}, respectively. These values are in good agreement with the experimental values of 1161 and 767 cm^{-1}, respectively, of gaseous CH_3SOH (*40*) even without scaling, confirming the appropriateness of the B3LYP/6-31G(d,p) level for the calculations presented here. Upon deuteration of the SOH group, the δSOD vibration occurred at a much lower frequency of 874 cm^{-1}, whereas the νSO frequency was affected little. In the sulfenate form, CH_3SO^-, νSO occurred at 836 cm^{-1}, which is 80 cm^{-1} higher than the νSO frequency of the protonated form (Table 1). After formation of S-bonded sulfenato

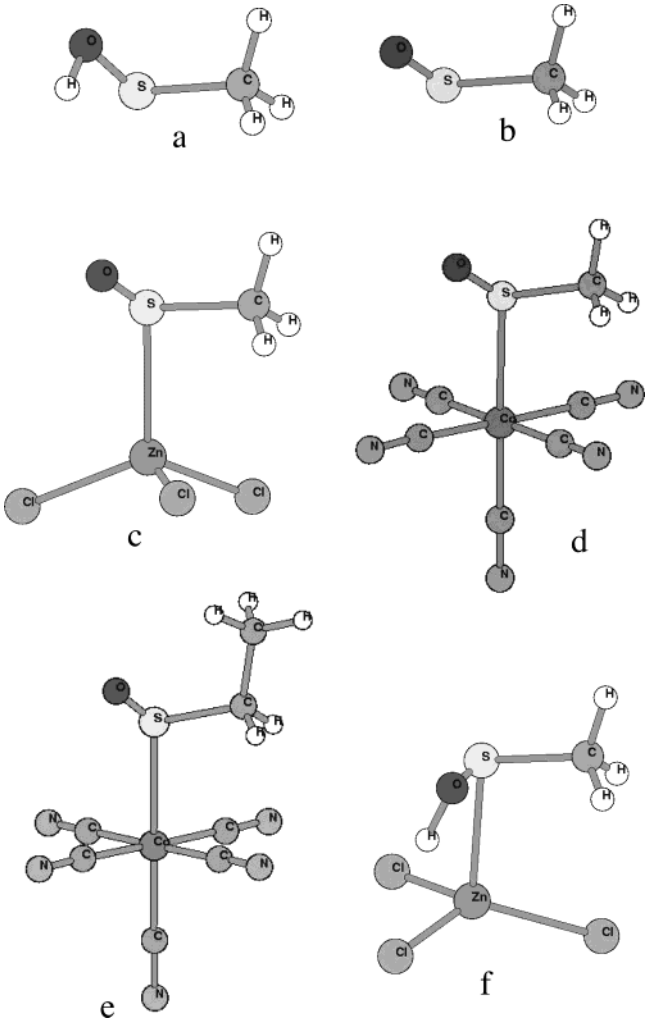

FIGURE 4: Optimized structures of methanesulfenic acid and the related compounds calculated as models of Cys-SO(H): (a) CH_3SOH, (b) CH_3SO^-, (c) $Zn(CH_3SO)Cl_3$, (d) $Co(CH_3SO)(CN)_5$, (e) $Co(CH_3CH_2SO)(CN)_5$, and (f) $Zn(CH_3SOH)Cl_3$.

complexes, the νSO frequencies further increased. In $Zn(CH_3SO)Cl_3$ (Figure 4c), the νSO mode occurred at 901 cm^{-1}. Although in $Co(CH_3SO)(CN)_5$ (Figure 4d) the νSO vibration splits into the two frequencies at 990 and 931 cm^{-1} by coupling with the CH_3 rocking vibration (ρCH_3), deuteration of the methyl group [$Co(CD_3SO)(CN)_5$] exhibited a single νSO frequency at 959 cm^{-1} (Table 1). In addition, a Co complex of ethanesulfenate, $Co(CH_3CH_2SO)(CN)_5$ (Figure 4e), exhibited a νSO vibration at a similar frequency of 934 cm^{-1}. These calculated frequencies of the sulfenato complexes are in good agreement with the experimental νSO frequencies of 1000−900 cm^{-1} in S-bonded sulfenato-Co (*41*) and sulfenato-Ni (*42*) complexes in the literature (Table 1). In a metal complex of protonated sulfenic acid, $Zn(CH_3SOH)Cl_3$ (Figure 4f), the νSO frequency was calculated to be 785 cm^{-1}, which is higher than the νSO frequency of free CH_3SOH but much lower than the frequencies of the deprotonated sulfenato complexes. The δSOH vibration of this complex appeared around 1360 cm^{-1} with split frequencies by coupling with δCH_3. The νSO vibrations in all the calculated compounds in Table 1 showed considerable downshifts of 5−10 cm^{-1} after ^{34}S isotope labeling, whereas the δSOH exhibited only a slight shift of −1 cm^{-1}.

The optimized geometries and calculated frequencies of CH_3SO_2H and its related compounds are presented in Figure 5 and Table 2. In CH_3SO_2H (Figure 5a), the protonated SO has single-bond character (S−O) while the other deprotonated SO has double-bond character (S═O). The νS═O and δSOH vibrations are coupled with each other and exhibited frequencies at 1190 (48% νS═O + 21% δSOH) and 1115 cm^{-1} (54% νS═O + 34% δSOH), and another νS−O vibration was calculated at a lower frequency of 719 cm^{-1} (Table 2). These frequencies are basically in agreement with the results of the recent calculation by Arsene at al. (*43*). Upon deuteration of the SO_2H group, the δSOD mode downshifts to 834 cm^{-1}, while the decoupled νS═O vibration is left at 1162 cm^{-1}. The νS−O frequency remained at 716 cm^{-1}, almost unchanged by this deuetration. The deprotonated sulfinate form, $CH_3SO_2^-$ (Figure 5b), exhibited two strong vibrations at 1105 and 1004 cm^{-1} arising from the asymmetric ($\nu_{as}SO_2$) and symmetric (ν_sSO_2) stretching modes, respectively. These frequencies are consistent with the experimental values of 1036 and 982 cm^{-1} obtained by the FTIR measurement of sodium methanesulfinate in a solid state (Table 2). In S-bonded sulfinato complexes, these νSO_2 frequencies upshifted similarly to the sulfenato complexes (see above). $Zn(CH_3SO_2)Cl_3$ (Figure 5c) exhibited frequencies at 1156 ($\nu_{as}SO_2$) and 1034 cm^{-1} (ν_sSO_2), and similar frequencies of 1152 ($\nu_{as}SO_2$) and 1032 cm^{-1} (ν_sSO_2) were obtained in $Co(CH_3SO_2)(CN)_5$. These calculated frequencies are in good agreement with the experimental values of 1250−1100 and 1100−1000 cm^{-1} for the $\nu_{as}SO_2$ and ν_sSO_2 vibrations, respectively, of $Co(CH_3SO_2)(CN)_5$ (*44*) and various S-bonded sulfinato complexes (*45*) (Table 2). νS═O and νS−O of protonated sulfinic acid and $\nu_{as}SO_2$ and ν_sSO_2 of free sulfinate and its metal complexes all exhibited relatively large ^{34}S shifts from −5 to −15 cm^{-1}.

In all the calculated sulfenic and sulfinic compounds, the νC−S modes occurred at 700−550 cm^{-1} (not shown), in agreement with the general group frequencies for the νC−S vibrations of sulfur compounds (*46*).

DISCUSSION

The light-induced FTIR difference spectrum of NHase between the dark inactive and light active forms exhibits two prominent signals at (1154−1148)(−)/1126(+) and (1040−1034)(−)/1019(+) cm^{-1} (Figures 2a and 3a). These signals downshifted to 1141(−)/1114(+) and 1026(−)/1012(+) cm^{-1} by 7−13/12 and 8−14/7 cm^{-1}, respectively, upon uniform ^{34}S labeling of NHase (Figures 2b and 3a, dotted line). The observed frequencies of 1154−1126 and 1040−1019 cm^{-1} are in good agreement with the calculated frequencies of 1156−1152 and 1034−1032 cm^{-1} for the $\nu_{as}SO_2$ and ν_sSO_2 vibrations, respectively, in the model sulfinato−Zn and sulfinato−Co complexes (panels c and d of Figure 5 and Table 2) as well as the frequency regions of 1250−1100 ($\nu_{as}SO_2$) and 1100−1000 cm^{-1} (ν_sSO_2) in various S-bonded sufinato complexes in the literature (*44*, *45*). In addition, the observed ^{34}S shifts (Figure 3a) are consistent with the calculated downshifts of 5−15 cm^{-1} for the sulfinato complexes (Table 2). In contrast, a free sulfinate anion ($CH_3SO_2^-$) exhibited lower frequencies of 1105 ($\nu_{as}SO_2$) and 1004 cm^{-1} (ν_sSO_2) in calculation and of 1036 ($\nu_{as}SO_2$) and 982 cm^{-1} (ν_sSO_2) in observation (Table 2).

Table 1: Calculated Frequencies and ^{34}S Shifts of the SO(H) Vibrations of Methanesulfenic Acid and the Related Compounds

	calculation (cm^{-1})		experimental	
	frequency[a]	$\Delta^{34}S$[b]	frequency (cm^{-1})	assignment[c]
CH_3SOH	1199 (44)	−1	1161[d]	δSOH
	756 (60)	−8	767[d]	νSO
CH_3SOD	874 (30)	0		δSOD
	753 (51)	−8		νSO
CH_3SO^-	836 (74)	−7		νSO
$Zn(CH_3SO)Cl_3$	901 (95)	−6		νSO
$Co(CH_3SO)(CN)_5$	990 (116), 931 (98)	−7, −5		νSO + ρCH_3
$Co(CD_3SO)(CN)_5$	959 (196)	−10		νSO
$Co(CH_3CH_2SO)(CN)_5$	934 (154)	−8		νSO
M(RSO)[e]			1000−900	νSO
$Zn(CH_3SOH)Cl_3$	1367 (39), 1358 (31)	−1, −1		δSOH + δCH_3
	785 (55)	−8		νSO

[a] Numbers in parentheses are IR intensities in km/mol. [b] Shifts by ^{34}S isotope change. [c] Abbreviations for the assignment: ν, stretching; δ, deformation; ρ, rocking. [d] Gaseous state of CH_3SOH [Köningshofen et al. (*40*)]. [e] S-bonded sulfenato−Co or sulfenato−Ni complexes [Adzamli et al. (*41*) and Grapperhaus and Darensbourg (*42*)].

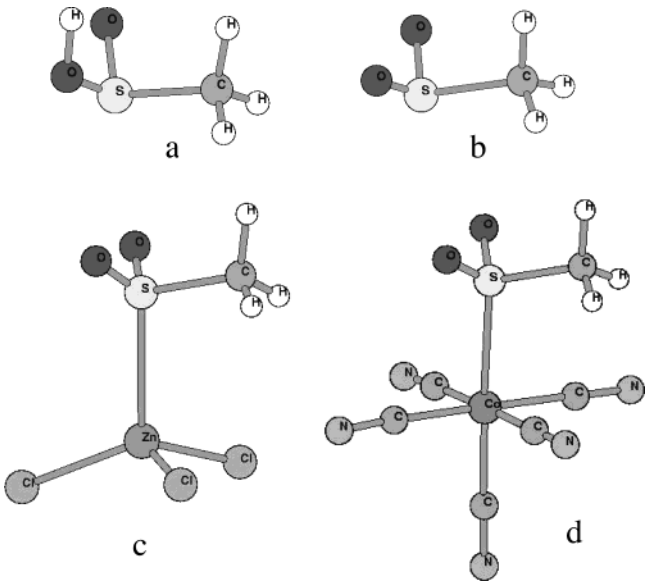

FIGURE 5: Optimized structures of methanesulfinic acid and the related compounds calculated as models of Cys-SO_2(H): (a) CH_3SO_2H, (b) $CH_3SO_2^-$, (c) $Zn(CH_3SO_2)Cl_3$, and (d) $Co(CH_3SO_2)(CN)_5$.

The DFT calculations showed that protonated methanesulfinic acid (CH_3SO_2H) also has two strong bands in the 1200−1000 cm^{-1} region that can be attributed to the coupled vibrations of νS═O and δSOH (Table 1). However, upon deuteration (CH_3SO_2D), only a single νS═O vibration was observed in this region due to decoupling of the downshifted δSOD vibration (Table 2). This drastic deuteration effect is clearly inconsistent with the observation that the prominent peaks were basically conserved in D_2O buffer with only slight (2−3 cm^{-1}) upshifts (Figure 3c).

All of these results indicate that the two prominent signals at (1154−1148)(−)/1126(+) and (1140−1134)(−)/1019(+) cm^{-1} are assigned to the $\nu_{as}SO_2$ and ν_sSO_2 vibrations, respectively, of the deprotonated αCys112-SO_2^- group bound to the Fe^{3+} center via the sulfur atom (Table 3). The differential shape of the signals means that both of the dark inactive and light active forms of NHase have a basically identical deprotonated structure of the αCys112-SO_2^- ligand with slight differences in its interactions. The downshifts of νSO_2^- frequencies upon the release of NO may be explained by the increase in the extent of π back-donation from the ferric ion to the SO_2^- group induced by elimination of the competitive π donation to NO.

Table 2: Calculated Frequencies and ^{34}S Shifts of the SO_2(H) Vibrations of Methanesulfinic Acid and the Related Compounds

	calculation (cm^{-1})		experimental frequency	
	frequency[a]	$\Delta^{34}S$[b]	(cm^{-1})	assignment[c]
CH_3SO_2H	1190 (121)	−9		νS═O + δSOH
	1115 (61)	−5		νS═O + δSOH
	719 (161)	−8		νS−O
CH_3SO_2D	1162 (135)	−12		νS═O
	834 (20)	−1		δSOD
	716 (153)	−8		νS−O
$CH_3SO_2^-$	1105 (225)	−14	1036[d]	$\nu_{as}SO_2$
	1004 (101)	−9	982[d]	ν_sSO_2
$Zn(CH_3SO_2)Cl_3$	1156 (192)	−15		$\nu_{as}SO_2$
	1034 (161)	−9		ν_sSO_2
$Co(CH_3SO_2)(CN)_5$	1152 (196)	−15	1150[e]	$\nu_{as}SO_2$
	1032 (234)	−9	1035[e]	ν_sSO_2
M(RSO_2)[f]			1250−1100	$\nu_{as}SO_2$
			1100−1000	ν_sSO_2

[a] Numbers in parentheses are IR intensities in km/mol. [b] Shifts by ^{34}S isotope change. [c] Abbreviations for the assignment: ν, stretching; δ, deformation; as, asymmetric; s, symmetric. [d] Solid CH_3SO_2Na (this study). [e] $K_3[Co(CH_3SO_2)(CN)_5]\cdot 2H_2O$ [Yamamoto et al. (*44*)]. [f] S-bonded sulfinato−metal complexes [Vitzthum and Lindner (*45*)].

Table 3: Vibrational Frequencies (cm^{-1}) and Assignments of the ^{34}S-Sensitive Bands in the Light-Induced FTIR Spectrum of NHase between the Dark Inactive and Light Active Forms

frequency ($\Delta^{34}S$[a])		
dark inactive NHase	light active NHase	assignment[b]
1154 (−13), 1148 (−7)	1126 (−12)	αCys112-SO_2^-, $\nu_{as}SO_2$
1040 (−14), 1034 (−5)	1019 (−7)	αCys112-SO_2^-, ν_sSO_2
915 (ca. −14)	908	αCys114-SO^-, νSO

[a] Shifts by ^{34}S isotope labeling. [b] Abbreviations for the assignment: ν, stretching; as, asymmetric; s, symmetric.

Another minor signal sensitive to ^{34}S labeling was found at 915(−)/908(+) cm^{-1} in the light-induced spectrum of NHase (Figure 3a,b). These frequencies best mach the νSO frequency of S-bonded sulfenato complexes, which showed νSO vibrations at 1000−900 cm^{-1} in the DFT calculation (Table 1) as well as in the experimental results in the literature (*41*, *42*). In addition, the ^{34}S shift of the 915 cm^{-1} peak of approximately −14 cm^{-1} is consistent with the calculated downshifts of 5−10 cm^{-1} in the sulfenato

complexes (Table 1). A free sulfenate anion (CH_3SO^-) exhibited a lower νSO frequency at 836 cm^{-1}, and protonated sulfenic acid (CH_3SOH) both in a free form and in an S-bonded complex exhibited νSO frequencies of <800 cm^{-1} (Table 1). The observed 915/908 cm^{-1} signal cannot originate from the δSOH vibrations, because only a slight deuteration effect was observed in this signal (Figure 3c,d) and δSOH should be rather insensitive to the ^{34}S isotope change (Table 1). In addition, in the metal complex of protonated sulfenic acid (Figure 4f), the δSOH vibration was calculated to occur at $\sim$1360 cm^{-1}, much higher than the value of 1199 cm^{-1} for free sulfenic acid (Table 1). Note that the medium-intensity signal at 1386/1370 cm^{-1} (Figure 2a) was basically unchanged by deuteration (data not shown), excluding the possibility of δSOH assignment. The 915/908 cm^{-1} signal is therefore reasonably assigned to the νSO vibration of the deprotonated αCys114-SO^- that is coordinated to the Fe^{3+} atom (Table 3). One concern for this assignment, however, is the weak intensity of the 915/908 cm^{-1} signal. This signal shows an intensity that is less than one-fourth of that of the major signals in the 1200−1000 cm^{-1} region (Figure 3a,b). The DFT calculations showed that the IR intensity of the sulfenate νSO is generally smaller than that of the sulfinate νSO_2 (Tables 1 and 2), but is not as small as the observed intensity. Coupling with the methylene (CH_2) vibrations in the Cys-SO^- anion, which could split the νSO intensity into a few coupled modes, was not seen in the calculation of the complex of ethanesulfenate, $Co(CH_3CH_2SO)(CN)_5$ (Figure 4e and Table 1). Also, formation of a hydrogen bond to the SO did not affect the calculated νSO intensity much (data not shown). One possible reason for this small intensity is that the frequency shift of the νSO band upon photoactivation of NHase is relatively small, and thus, the difference spectrum provides only a weak intensity. The possibility that the deprotonated and protonated forms of sulfenic acid are in equilibrium at pH 7.5, the situation which provides only a partial sulfenate population, is unlikely, because the relative intensity of the 915/908 cm^{-1} signal was basically unchanged in the pH range from 5.5 to 11.0 (data not shown).

Thus, the αCys114-SOH is most likely in a deprotonated Cys-SO^- form. Nevertheless, the possibility of the protonated form cannot be totally excluded, because its νSO band that is expected to appear below 800 cm^{-1} could not be observed in these FTIR spectra, and the δSOH band located at a higher frequency (>1100 cm^{-1}) may be difficult to detect because of the weak intensity and a small ^{34}S effect (Table 1).

The above conclusion that αCys112-SO_2H and most likely αCys114-SOH have deprotonated Cys-SO_2^- and Cys-SO^- structures, respectively (Table 3), is consistent with the structures of the model compounds of the active site of NHase (*47*−*50*) and those of various S-bonded sulfinato and sulfenato complexes (*41*, *42*, *44*, *45*). The crystal structures and the νSO_2 and νSO frequencies showed that the sulfinic and sulfenic groups in these compounds are all deprotonated in the metal complexes. In addition, the results of this study are consistent with the theoretical study by Greene et al. (*51*), in which the DFT and INDO/S calculations assuming the iron center with deprotonated sulfinate and sulfenate ligands reproduced well the geometry of the X-ray structure and the electronic absorption spectrum of dark inactive NHase.

The parallel upshifts by 2−3 cm^{-1} of the two prominent signals in the 1200−1000 cm^{-1} region upon deuteration (Figure 3) indicate that the oxygen atoms of αCys112-SO_2^- are hydrogen-bonded with exchangeable protons. This is consistent with the X-ray structure of inactive NHase, in which hydrogen bond interactions of the sulfinic group with βArg56 and βArg141 were predicted (Figure 1) (*10*). The crystal structure of dark inactive NHase also showed that a water molecule is located in the distance that can form a hydrogen bond with the SO_2 at the oxygen atom on the NO side (*52*). The deprotonated Cys-SO_2^- structure indicates that both the Arg side chains and the water molecules work to donate protons to the oxygen atoms of the SO_2 group. Furthermore, hydrogen bonding of αCys112-SO_2^- with the Arg side chains is consistent with the frequency shifts of the SO_2 bands at (1154−1148)/1126 and (1140−1034)/1019 cm^{-1} to 1157/1134 and 1045/1026 cm^{-1}, respectively, by mutation of βArg56 to Lys (*53*). On the other hand, the 915/908 cm^{-1} peaks seemed to slightly downshift by 1−3 cm^{-1} upon deuteration, although this deuteration effect may not be very accurate because of the small intensities and the overlap of other bands (Figure 3a,c). According to the X-ray structure, the αCys114-SO^- must be hydrogen bonded with the βArg56 side chain (Figure 1) (*10*). In this hydrogen bond, the guanidinium group of βArg56 may donate a proton to the deprotonated S−O bond. In addition, a water or hydroxide ligand to the iron center (*12*, *15*, *16*) could serve to donate a proton to either the SO or the SO_2 group in the light active form in the absence of substrate.

It has been shown that the presence of the Cys-SO_2^- and Cys-SO^- groups as the ligands of the metal center is crucial to the enzymatic activity of NHase (*21*, *30*, *54*). One of the roles of these groups is clearly to form a reactive cavity at the interface of the α and β subunits via hydrogen bond interactions with the βArg56 and βArg141 residues. Another role may be manipulating the electronic property of the iron center. Recent theoretical calculations showed the effects of the oxidized Cys ligands on the electronic structure of the iron center, suggesting the significance in the NO-related photosensitivity and the catalytic activity (*51*, *55*). A more direct role of the Cys-SO_2^- and Cys-SO^- groups in the catalytic reaction is also possible. Two distinct mechanisms have been proposed for nitrile hydration in NHase (*14*). (1) A nitrile substrate is attached to the non-heme iron, which works as a Lewis acid to activate the nitrile, and the nucleophilic attack of a water molecule to the nitrile carbon occurs. (2) A metal-bound water or hydroxide ion either attacks the nitrile carbon or activates a water molecule, which in turn can act as a nucleophile. Direct ligation of the nitrile substrate was supported by modeling of a substrate analogue, iodoacetonitrile, in the binding pocket of the X-ray structure of the active NHase based on the iodine position (*14*). The ESR study of NHase by Sugiura et al. (*12*) also suggested that a nitrile substrate is bound to the iron center. In the studies of the model compounds of the active center of NHase, Shearer et al. (*56*) synthesized nitrile-bound Fe complexes that exhibit spectroscopic properties similar to those of NHase, supporting the nitrile binding mechanism, whereas Noveron et al. (*57*) supported the metal-bound hydroxide mechanism by synthesis of the model Co−NHase complex that showed the function of nitrile hydration at alkaline pH. Provided that the nitrile−ligand model exists, one can speculate that a water molecule is hydrogen bonded to either Cys-SO_2^- or Cys-SO^-, increasing the basicity of

the water oxygen to facilitate nucleophilic attack on the nitrile. Also, in the context of the second model, the water molecule bound to one of these groups could be further activated by the interaction with the metal-bound hydroxide for the attack on the nitrile. The water molecule hydrogen bonded to the oxygen of Cys-SO_2^-, which was detected by X-ray crystallography, can be a candidate for this active water (*52*). However, this water molecule is structurally rigid between the SO_2 and βTyr76, and thus can be important in constructing the structure of the active site of NHase rather than as a reactant water. On the other hand, there is a space above the Cys-SO^- group, where unstable water can be located. Since one of the two lone pairs of the SO oxygen is free, it is possible that the active water molecule is hydrogen bonded to this SO site and attacks the Fe-bound nitrile. The significant role of the Cys-SO^- is consistent with the fact that further oxidation of this group to Cys-SO_2^-, which may not change the cavity structure but will affect the electronic property of the oxygen atom, makes the NHase inactive (*30*).

REFERENCES

1. Kobayashi, M., Nagasawa, T., and Yamada, H. (1992) *Trends Biotechnol. 10*, 402−408.
2. Yamada, H., and Kobayashi, M. (1996) *Biosci. Biotechnol. Biochem. 60*, 1391−1400.
3. Kobayashi, M., and Shimizu, S. (1998) *Nat. Biotechnol. 16*, 733−736.
4. Nakajima, T., Doi, T., Satoh, Y., Fujimura, A., and Watanabe, I. (1987) *Chem. Lett.*, 1767−1770.
5. Nagamune, T., Kurata, H., Hirata, M., Honda, J., Hirata, A., and Endo, I. (1990) *Photochem. Photobiol. 51*, 87−90.
6. Noguchi, T., Honda, J., Nagamune, T., Sasabe, H., Inoue, Y., and Endo, I. (1995) *FEBS Lett. 358*, 9−12.
7. Noguchi, T., Hoshino, M., Tsujimura, M., Odaka, M., Inoue, Y., and Endo, I. (1996) *Biochemistry 35*, 16777−16781.
8. Odaka, M., Fujii, K., Hoshino, M., Noguchi, T., Tsujimura, M., Nagashima, S., Yohda, M., Nagamune, T., Inoue, Y., and Endo, I. (1997) *J. Am. Chem. Soc. 119*, 3785−3791.
9. Bonnet, D., Artaud, I., Moali, C., Petre, D., and Mansuy, D. (1997) *FEBS Lett. 409*, 216−220.
10. Nagashima, S., Nakasako, M., Dohmae, N., Tsujimura, M., Tokio, K., Odaka, M., Yohda, M., Kamiya, N., and Endo, I. (1998) *Nat. Struct. Biol. 5*, 347−351.
11. Scarrow, R. C., Strickler, B. S., Ellison, J. J., Shoner, S. C., Kovacs, J. A., Cummings, J. G., and Nelson, M. J. (1998) *J. Am. Chem. Soc. 120*, 9237−9245.
12. Sugiura, Y., Kuwahara, J., Nagasawa, T., and Yamada, H. (1987) *J. Am. Chem. Soc. 109*, 5848−5850.
13. Popescu, V. C., Münck, E., Fox, B. G., Sanakis, Y., Cummings, J. G., Turner, I. M., and Nelson, M. J. (2001) *Biochemistry 40*, 7984−7991.
14. Huang, W. J., Jia, J., Cummings, J., Nelson, M., Schneider, G., and Lindqvist, Y. (1997) *Structure 5*, 691−699.
15. Jin, H., Turner, I. M., Jr., Nelson, M. J., Gurbiel, R. J., Doan, P. E., and Hoffman, B. M. (1993) *J. Am. Chem. Soc. 115*, 5290−5291.
16. Doan, P. E., Nelson, M. J., Jin, H., and Hoffmann, B. M. (1996) *J. Am. Chem. Soc. 118*, 7014−7015.
17. Nelson, M. J., Jin, H., Turner, I. M., Grove, G., Scarrow, R. C., Brennan, B. A., and Que, L., Jr. (1991) *J. Am. Chem. Soc. 113*, 7072−7073.
18. Scarrow, R. C., Brennan, B. A., Cummings, J. G., Jin, H., Duong, D. J., Kindt, J. T., and Nelson, M. J. (1996) *Biochemistry 35*, 10078−10088.
19. Brennan, B. A., Cummings, J. G., Chase, D. B., Turner, I. M., and Nelson, M. J. (1996) *Biochemistry 35*, 10068−10077.
20. Tsujimura, M., Dohmae, N., Odaka, M., Chijimatsu, M., Takio, K., Yohda, M., Hoshino, M., Nagashima, S., and Endo, I. (1997) *J. Biol. Chem. 272*, 29454−29459.
21. Murakami, T., Nojiri, M., Nakayama, H., Odaka, M., Yohda, M., Dohmae, N., Takio, K., Nagamune, T., and Endo, I. (2000) *Protein Sci. 9*, 1024−1030.
22. Bonnet, D., Stevens, J. M., de Sousa, R. A., Sari, M. A., Mansuy, D., and Artaud, I. (2001) *J. Biochem. 130*, 227−233.
23. Miyanaga, A., Fushinobu, S., Ito, K., and Wakagi, T. (2001) *Biochem. Biophys. Res. Commun. 288*, 1169−1174.
24. Claiborne, A., Mallett, T. C., Yeh, J. I., Luba, J., and Parsonage, D. (2001) *Adv. Protein Chem. 58*, 215−276.
25. Claiborne, A., Yeh, J. I., Mallett, T. C., Luba, J., Crane, E. J., Charrier, V., and Parsonage, D. (1999) *Biochemistry 38*, 15407−15416.
26. Claiborne, A., Miller, H., Parsonage, D., and Ross, R. P. (1993) *FASEB J. 7*, 1483−1490.
27. Giles, N. M., Giles, G. I., and Jacob, C. (2003) *Biochem. Biophys. Res. Commun. 300*, 1−4.
28. Fu, X., Kassim, S. Y., Parks, W. C., and Heinecke, J. W. (2001) *J. Biol. Chem. 276*, 41279−41287.
29. Woo, H. A., Chae, H. Z., Hwang, S. C., Yang, K. S., Kang, S. W., Kim, K., and Rhee, S. G. (2003) *Science 300*, 653−656.
30. Tsujimura, M., Odaka, M., Nakayama, H., Dohmae, N., Koshino, H., Asami, T., Hoshino, M., Takio, K., Yoshida, S., Maeda, M., and Endo, I. (2003) *J. Am. Chem. Soc.* (in press).
31. Tsujimura, M., Odaka, M., Nagashima, S., Yohda, M., and Endo, I. (1996) *J. Biochem. 119*, 407−413.
32. Frisch, M. J., Trucks, G. W., Schlegel, H. B., Scuseria, G. E., Robb, M. A., Cheeseman, J. R., Zakrzewski, V. G., Montgomery, J. A., Stratmann, R. E., Burant, J. C., Dapprich, S., Millam, J. M., Daniels, A. D., Kudin, K. N., Strain, M. C., Farkas, O., Tomasi, J., Barone, V., Cossi, M., Cammi, R., Mennucci, B., Pomelli, C., Adamo, C., Clifford, S., Ochterski, J., Petersson, G. A., Ayala, P. Y., Cui, Q., Morokuma, K., Malick, D. K., Rabuck, A. D., Raghavachari, K., Foresman, J. B., Cioslowski, J., Ortiz, J. V., Stefanov, B. B., Liu, G., Liashenko, A., Piskorz, P., Komaromi, I., Gomperts, R., Martin, R. L., Fox, D. J., Keith, T., Al-Laham, M. A., Peng, C. Y., Nanayakkara, A., Gonzalez, C., Challacombe, M., Gill, P. M. W., Johnson, B. G., Chen, W., Wong, M. W., Andres, J. L., Head-Gordon, M., Replogle, E. S., and Pople, J. A. (1998) *Gaussian 98*, revision A.7, Gaussian, Inc., Pittsburgh, PA.
33. Becke, A. D. (1993) *J. Chem. Phys. 98*, 5648−5652.
34. Lee, C., Yang, W., and Parr, R. G. (1988) *Phys. Rev. B 37*, 785−789.
35. Shimanouchi, T. (1968) *Computer Programs of Normal Coordinate Treatment of Polyatomic Molecules*, The University of Tokyo, Tokyo.
36. Byler, D. M., and Susi, H. (1986) *Biopolymers 25*, 469−487.
37. Haris, P. I., and Chapman, D. (1992) *Trends Biol. Sci. 17*, 328−333.
38. Braiman, M. S., Briercheck, D. M., and Kriger, K. M. (1999) *J. Phys. Chem. B 103*, 4744−4750.
39. Kopf, M. A., Bonnet, D., Artaud, I., Petre, D., and Mansuy, D. (1996) *Eur. J. Biochem. 240*, 239−244.
40. Königshofen, A., Behnke, M., Hoverath, M., and Hahn, J. (1999) *Z. Anorg. Allg. Chem. 625*, 1779−1786.
41. Adzamli, I. K., Libson, K., Lydon, J. D., Elder, R. C., and Deutsch, E. (1979) *Inorg. Chem. 18*, 303−311.
42. Grapperhaus, C. A., and Darensbourg, M. Y. (1998) *Acc. Chem. Res. 31*, 451−459.
43. Arsene, C., Barnes, I., Becker, K. H., Schneider, W. F., Wallington, T. T., Mihalopoulos, N., and Patroescu-Klotz, I. V. (2002) *Environ. Sci. Technol. 36*, 5155−5163.
44. Yamamoto, K., Syono, T., and Shinra, K. (1967) *J. Chem. Soc. Jpn. 88*, 958−960.
45. Vitzthum, G., and Lindner, E. (1971) *Angew. Chem., Int. Ed. 10*, 315−326.
46. Socrates, G. (1994) in *Infrared Characteristic Group Frequencies*, 2nd ed., pp 161−172, John Wiley & Sons, Chichester, U.K.
47. Mascharak, P. K. (2002) *Coord. Chem. Rev. 225*, 201−214.
48. Kung, I., Schweitzer, D., Shearer, J., Taylor, W. D., Jackson, H. L., Lovell, S., and Kovacs, J. A. (2000) *J. Am. Chem. Soc. 122*, 8299−8300.
49. Rat, M., de Sousa, R. A., Vaissermann, J., Leduc, P., Mansuy, D., and Artaud, I. (2001) *J. Inorg. Biochem. 84*, 207−213.
50. Heinrich, L., Mary-Verla, A., Li, Y., Vaissermann, J., and Chottard, J. C. (2001) *Eur. J. Inorg. Chem.*, 2203−2206.
51. Greene, S. N., Chang, C. H., and Richards, N. G. J. (2002) *Chem. Commun.*, 2386−2387.
52. Nakasako, M., Odaka, M., Yohda, M., Dohmae, N., Takio, K., Kamiya, N., and Endo, I. (1999) *Biochemistry 38*, 9887−9898.

53. Piersma, S. R., Nojiri, M., Tsujimura, M., Noguchi, T., Odaka, M., Yohda, M., Inoue, Y., Ambe, F., and Endo, I. (2000) *J. Inorg. Biochem. 80*, 283−288.
54. Nojiri, M., Nakayama, H., Odaka, M., Yohda, M., Takio, K., and Endo, I. (2000) *FEBS Lett. 465*, 173−177.
55. Nowak, W., Ohtsuka, Y., Hasegawa, J., and Nakatsuji, H. (2002) *Int. J. Quantum Chem. 90*, 1174−1187.
56. Shearer, J., Jackson, H. L., Schweitzer, D., Rittenberg, D. K., Leavy, T. M., Kaminsky, W., Scarrow, R. C., and Kovacs, J. A. (2002) *J. Am. Chem. Soc. 124*, 11417−11428.
57. Noveron, J. C., Olmstead, M. M., and Mascharak, P. K. (1999) *J. Am. Chem. Soc. 121*, 3553−3554.

BI035260I